Received: 28 July 2021 | Accepted: 25 September 2021

DOI: 10.1111/gcb.15939

Global Change Biology WILEY

PRIMARY RESEARCH ARTICLE

Quantitatively monitoring the resilience of patterned vegetation in the Sahel

Joshua E. Buxton[1] | Jesse F. Abrams[1,2] | Chris A. Boulton[1] | Nick Barlow[3] | Camila Rangel Smith[3] | Samuel Van Stroud[3,4] | Kirsten J. Lees[1] | Timothy M. Lenton[1]

[1]Global Systems Institute, University of Exeter, Exeter, UK

[2]Institute for Data Science and Artificial Intelligence, University of Exeter, Exeter, UK

[3]The Alan Turing Institute, London, UK

[4]Department of Physics and Astronomy, University College London, London, UK

Correspondence
Joshua E. Buxton, Global Systems Institute, University of Exeter, Exeter, EX4 4QE, UK.
Email: j.buxton@exeter.ac.uk

Funding information
The Leverhulme Trust, Grant/Award Number: RPG-2018-046; The Alan Turing Institute, Grant/Award Number: R-EXE-001; UCL CDT in Data Intensive Science, Grant/Award Number: ST/P006736/1

Abstract

Patterning of vegetation in drylands is a consequence of localized feedback mechanisms. Such feedbacks also determine ecosystem resilience—i.e. the ability to recover from perturbation. Hence, the patterning of vegetation has been hypothesized to be an indicator of resilience, that is, spots are less resilient than labyrinths. Previous studies have made this qualitative link and used models to quantitatively explore it, but few have quantitatively analysed available data to test the hypothesis. Here we provide methods for quantitatively monitoring the resilience of patterned vegetation, applied to 40 sites in the Sahel (a mix of previously identified and new ones). We show that an existing quantification of vegetation patterns in terms of a feature vector metric can effectively distinguish gaps, labyrinths, spots, and a novel category of spot–labyrinths at their maximum extent, whereas NDVI does not. The feature vector pattern metric correlates with mean precipitation. We then explored two approaches to measuring resilience. First we treated the rainy season as a perturbation and examined the subsequent rate of decay of patterns and NDVI as possible measures of resilience. This showed faster decay rates—conventionally interpreted as greater resilience—associated with wetter, more vegetated sites. Second we detrended the seasonal cycle and examined temporal autocorrelation and variance of the residuals as possible measures of resilience. Autocorrelation and variance of our pattern metric increase with declining mean precipitation, consistent with loss of resilience. Thus, drier sites appear less resilient, but we find no significant correlation between the mean or maximum value of the pattern metric (and associated morphological pattern types) and either of our measures of resilience.

KEYWORDS
Africa, drylands, patterned vegetation, resilience, Sahel

1 | INTRODUCTION

Ecosystems with strong internal feedback mechanisms can exhibit multiple stable states. Abrupt changes, known as regime shifts, can occur when such systems pass a tipping point and transition from one stable state to another (Scheffer et al., 2001). Once a system has transitioned to a new stable state, it is usually difficult to reverse this transition, due to hysteresis. Hence, regime shifts can have severe consequences for those who depend upon an ecosystem. Predicting tipping points in complex systems is difficult because of their inherent nonlinearity. However, a growing body of work has shown that the phenomenon of 'critical slowing down' prior to a tipping point can give generic early warning signals (Dakos et al., 2008; Lenton, 2011; Scheffer et al., 2009). In essence, a system becomes slower at recovering from short-term fluctuations before it undergoes an abrupt shift. This is because under steady forcing, the restoring negative feedbacks that maintain the original state get weaker before strong positive feedbacks take over at the tipping point. This precursor signal is often referred to in ecology as 'loss of resilience'—where resilience is defined as the rate at which a system recovers to its initial state after perturbation (Pimm, 1984).

Multiple metrics have been employed to measure changes in resilience. Where individual perturbations can be clearly identified, the response time of a system to return back to its initial state can be directly measured (Lees et al., 2020; Pimm, 1984). Where a system is subject to continual stochastic perturbations ('noise'), increasing temporal autocorrelation (e.g. lag-1 autocorrelation; AR(1)) (Dakos et al., 2008) and increasing variance (Scheffer et al., 2009) signal loss of resilience. Spatial equivalents of these temporal signals can also be used (Kéfi et al., 2014). Due to the difficulty in obtaining frequent, high-quality spatial data and the high levels of computational power required to analyse it, most studies focus solely upon spatially aggregated data for time-series analysis of systems to analyse their resilience. This difficulty can be mitigated using space-for-time substitutions (Kéfi et al., 2014; Verbesselt et al., 2016). Other spatial resilience studies are often conducted with modelled data (Chen et al., 2015; Siero et al., 2019) or in laboratory conditions (Dai et al., 2013). Kéfi et al. (2014) suggest that a combination of spatial pattern analysis with temporal analysis can improve our understanding of system resilience.

Dryland patterned vegetation belongs to a special class of reaction–diffusion systems, first recognized by Alan Turing (1952), where feedback gives rise to regular spatial patterns. The patterns result from an interplay of a local facilitation mechanism; here plants retain water, and a more distant competition mechanism; this denies other plants water (Barbier et al., 2006; HilleRisLambers et al., 2001). Typically patterns transition from 'gaps' to 'labyrinths' to 'spots' as rainfall declines—then vegetation reaches a tipping point—abruptly disappearing below a critical rainfall level (Meron et al., 2004). Furthermore, different pattern morphologies affect the ability of the system to conserve resources (Mayor et al., 2013). Consequently, in patterned systems, the pattern itself may act as a visual indicator of the changing balance of feedbacks—leading to the hypothesis that the pattern could act as a resilience indicator of proximity to a tipping point (Kéfi et al., 2014; Rietkerk et al., 2004). However, Dakos et al. (2011) find that different models of vegetation patterning give qualitatively different results for how resilience varies approaching a tipping point. In particular, a 'scale-dependent feedback' pattern vegetation model displays slowing down prior to a tipping point, but AR(1) does not increase as the pattern morphology transitions. Hence, we set out to test the hypothesis of a link between vegetation pattern and resilience with remotely sensed data.

Here, we focus on patterned vegetation in the Sahel, this region extends across Northern Africa from Mauritania in the west through to Chad and central Sudan in the east. The region is characterized by low levels of rainfall (Le Houérou, 1989), depleted soils (Sanchez, 2002), increasing use of marginal lands (Doso, 2014), weak states and institutions (Raleigh, 2010), extreme poverty (Beegle & Christiaensen, 2019), a growing population (May et al., 2017) and degradation of land and resources during times of drought (IPBES, 2018). The Sahel became a region of international concern following the severe droughts and famines of the late 1960s and 1970s. It was thought that this would lead to the southwards expansion of the Sahara desert and provoked a broader discussion about desertification (Helldén, 1991; Nicholson et al., 1998). The changes affecting the precipitation regime and the vegetation across the Sahel were seen, by some, as irreversible (Charney, 1975) and led to the development of the United Nations Convention to Combat Desertification (Hermann & Hutchinson, 2005). Subsequent changes in precipitation and the apparent recovery of vegetation in parts of the Sahel have caused much debate about the wider resilience of Sahelian vegetation to precipitation changes (Hermann & Hutchinson, 2005; Kusserow, 2017).

The pronounced North–South precipitation gradient of the Sahel (Le Houérou, 1989) enables the formation of vegetation patterns of diverse morphologies, including gaps, labyrinths and spots (Deblauwe et al., 2008; Mander et al., 2017; Trichon et al., 2018), as seen in Figure 1. Some of these patterns have previously been studied within the context of wider Sahelian precipitation trends and human influence (Barbier et al., 2006; Leblanc et al., 2008). Trichon et al. (2018) present evidence of vegetation patterns undergoing degradation and decline during Sahelian drought periods, with some recovery observed following the increase in rainfall. This recovery is limited to areas of higher precipitation, with northern sites undergoing less recovery. It is suggested that this is due to lower precipitation sites displaying lower resilience and therefore having proceeded past a tipping point during the drought (Trichon et al., 2018). Model studies have shown that in addition to changes in rainfall, overgrazing can decrease the resilience of patterned vegetation and induce tipping points at rainfall levels that would otherwise be stable (Siero et al., 2019).

Few quantitative measures of pattern vegetation are available; these include Fourier analysis (Couteron, 2002; Penny et al., 2013), Shannon entropy (Konings et al., 2011) and morphometric analysis (Mander et al., 2017). Due to the necessity of having high-resolution data to perform these analyses, few studies have quantified changes

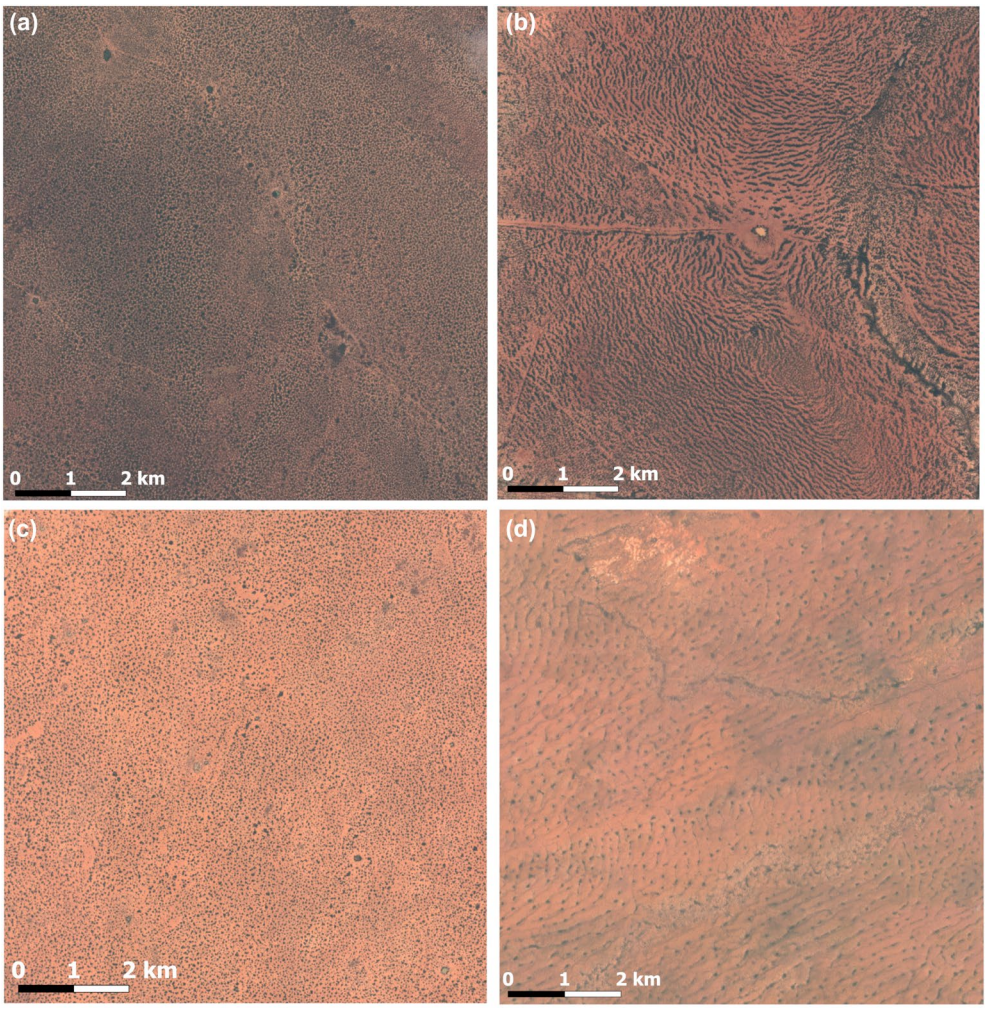

FIGURE 1 Examples of the four classes of pattern vegetation site analysed in this study. (a) Gaps, ID: 02, 10-2016. (b) Labyrinths, ID: 01, 10-2016. (c) Spots, ID: 00, 10-2016. (d) Spot/Labyrinths, ID: 28, 09-2017. All images are of the (cloud free) peak cover of the vegetation within a seasonal cycle

in patterned vegetation. Existing studies rely on infrequent historical aerial data (Trichon et al., 2018) or consider the changes in vegetation at certain time points relating to human intervention, such as road construction (Gowda et al., 2018) or firewood collection and land-use change (Leblanc et al., 2008). We build upon the method presented in Mander et al. (2017) and offer a novel way of continued monitoring of patterned vegetation sites and their response to precipitation. Satellite imagery from Sentinel-2 has the potential to provide high-resolution data over large areas of land at a frequent time step, thereby enabling the changes in pattern vegetation to be analysed across regions.

Here we examine the utility of morphological analysis to distinguish between patterned vegetation classes and the relationship between these patterns and precipitation. We apply our vegetation pattern metric to understand the resilience of patterned vegetation and which factors, such as morphology and rainfall level, affect this resilience. We measure resilience as decay rate following a perturbation, and in terms of AR(1) and variance. We also investigate the spatial distribution of pattern trends across the Sahel in the context of the North–South rainfall gradient and changes in the East–West precipitation regime (Nicholson et al., 2018).

2 | METHODS

In this study, we utilize a remotely sensed resilience monitoring Python toolkit for patterned vegetation, with an initial focus on drylands, called *pyveg* (Barlow et al., 2020). This draws on a number of existing tools and insights. It requires (1) a source of remotely sensed data of patterned vegetation, derived from the Sentinel-2 satellite accessed through Google Earth Engine (GEE); (2) a method of turning the qualitative observation of pattern into a quantitative metric called Offset50, based upon feature vector analysis used in Mander et al. (2017); and (3) additional data on the potential environmental determinants of resilience, using precipitation data from the ERA5 dataset.

2.1 | Sites of patterned vegetation

We reviewed existing literature for sites across the Sahel that were characterized by patterned vegetation. We considered a wider range of locations, of an initial 56 sites (8.5 km × 8.5 km in size) and filtered the sites selected for analysis down to 40 sites, as shown in Table 1, based on several criteria. Some initial sites in northern Africa had two rainy seasons per year and were therefore not true Sahelian sites, other historical sites that were reported in the literature were removed as they had suffered such significant degradation that the vegetation morphology was unclear or occupied very small areas, such as a tiger bush and dotted vegetation site in Burkina Faso (Leprun, 1999). Other sites were removed due to unclear vegetation patterning or incorrect labelling (see Table S1 for full list) or due to outliers linked to too small vegetation to be recorded (Figure S4). Of the sites considered as part of this analysis, 13 are in Mali, 2 in Mauritania, 5 in Niger, 1 in Nigeria, 4 in Senegal and 15 in Sudan (Figure 2 and Table 1). The chosen sites represent a mix of different types of patterned vegetation with 7 sites demonstrating gaps, 12 demonstrating labyrinths and 11 demonstrating spots (examples of these are given in Figure 1). In addition to these recognized vegetation patterns, we include sites which we call 'spot–labyrinths', these patterns seem to be highly dependent on precipitation and have more dramatic annual changes than spots or labyrinths. The form that these patterns take post-precipitation is determined by the landscape, with the precipitation that collects in small channels and gullies enabling the spread of this vegetation (an example of the topography of this region is provided in Figure S3). In the dry season, the 'spot–labyrinth' patterns often appear to be isolated, highly degraded spots. However, following the rainy season, the vegetation will spread across the landscape and form 'labyrinth-esque' patterns. There are 10 of these 'spot–labyrinth' sites. They are included due to their resemblance to other vegetation patterns and rapid changes across their annual cycles. The pattern morphology of sites was classified by inspection by considering the images of the sites across the whole time series, with particular focus given to the fullest extent of vegetation following a rainy season. This was done by two researchers initially, before consensus was gained from the rest of the authors.

2.2 | Satellite data and preliminary data processing

The data used in this analysis were taken from the Sentinel-2 satellite, which captures remotely sensed data with a resolution of 10m with its multispectral imager (MSI) (Drusch et al., 2012). This resolution provides enough clarity to visualize vegetation patterning. For the purpose of this study, Sentinel-2 data from January 2016 to December 2019 were extracted from Google Earth Engine (GEE), a data repository and cloud computing service (Gorelick et al., 2017). Large-scale data analysis was undertaken using the Microsoft Azure Cloud computing service.

Our data processing workflow is as follows and is outlined in Figure 3. We start preliminary data processing by creating monthly median composites of the multi-band Sentinel-2 data. This is done to remove extreme pixel values caused by clouds, air pollution and sun angle. From these monthly multi-band images, two sets of images are constructed; Red-Green-Blue (RGB) images and Normalized Difference Vegetation Index (NDVI) images. NDVI is a measure of plant health and is connected to the level of chlorophyll in plant leaves (Rouse et al., 1974), it is calculated from multispectral images using the near-infrared (NIR) band and the red band (RED), and is defined as:

$$\mathrm{NDVI} = \left(\frac{\mathrm{NIR} - \mathrm{RED}}{\mathrm{NIR} + \mathrm{RED}}\right) \tag{1}$$

These NDVI images are rescaled from the original −1 to 1 in order to fit a 0–255 greyscale. Prior to the morphological analysis of vegetation patterns, several image enhancement steps occur for the greyscale NDVI images. Image contrast is increased through histogram equalization, these images then undergo adaptive thresholding to classify vegetation pixels as black and background pixels as white. This adaptive thresholding step calculates the mean brightness of a 51 × 51 pixel block around each pixel, and offsets this value by 5 to create the soil-vegetation threshold. Median filtering is also applied to reduce noise within the image. Once processed, these images are then divided into a 17 × 17 grid of 50 × 50 pixel sub-images, these sub-images contain the same number of pixels as those used in Mander et al. (2017).

Sub-image patterned vegetation is quantified using the network centrality calculation first described in Mander et al. (2017). A graph with vertices corresponding to each pixel is formed for each binary sub-image. If a vegetation pixel falls within a 3 × 3 neighbourhood of another, then an edge connects the corresponding two vertices. These graph vertices are then ranked using subgraph centrality (SC) (Estrada and Rodríguez-Velázquez, 2005). For some vertex v, with a non-negative integer l, where u_l is the number of closed walks with length l which begin at v, the centrality of the vertex v is given by:

$$\mathrm{SC}(v) = \sum_{l=1}^{\infty} \frac{u_l(v)}{l!} \tag{2}$$

This can be calculated using eigenvalues and eigenvectors of the graph's adjacency matrix. These vertices are then collected into a sequence of expanding subregions based upon their subgraph centrality rank. In total, 20 of these subgraphs are formed, beginning with the top 5% vertices, with the groups then expanded by each 5% increment. A graph, designated G, to describe each subregion is composed of each connected component. We define the Euler characteristic of a subregion as:

$$\chi(G) = V - E \tag{3}$$

TABLE 1 Table of patterned vegetation sites included in this study

ID	Country	Latitude	Longitude	Type	Source
0	Sudan	11.58	27.94	Spots	Mander et al. (2017)
1	Sudan	11.12	28.37	Labyrinths	Mander et al. (2017)
2	Sudan	10.96	28.2	Gaps	Mander et al. (2017)
3	Niger	13.12	2.59	Labyrinths	Valentin and d'Herbès (1999)
4	Niger	13.17	1.58	Labyrinths	Valentin and d'Herbès (1999)
5	Senegal	15.2	−15.2	Labyrinths	Deblauwe et al. (2008)
6	Senegal	15.09	−15.04	Labyrinths	Deblauwe et al. (2008)
7	Senegal	15.8	−14.36	Gaps	De Wispelaere (1980)
8	Senegal	15.11	−14.53	Gaps	De Wispelaere (1980)
16	Mali	15.03	−0.87	Spot–labyrinths	Leprun (1999)
18	Mali	15.34	−1.15	Spot–labyrinths	Leprun (1999)
20	Mali	14.85	−1.43	Spot–labyrinths	Leprun (1999)
21	Mali	14.97	−1.12	Spot–labyrinths	Leprun (1999)
23	Mali	15.02	−1.35	Spot–labyrinths	Deblauwe et al. (2008) (by inspection)
25	Mali	16.19	−1.83	Spot–labyrinths	Deblauwe et al. (2008) (by inspection)
26	Mali	16.17	−2.03	Spot–labyrinths	Deblauwe et al. (2008) (by inspection)
27	Mali	16.48	−1.87	Spot–labyrinths	Deblauwe et al. (2008) (by inspection)
28	Mali	15.95	−1.52	Spot–labyrinths	Deblauwe et al. (2008) (by inspection)
29	Mali	15.86	−2.05	Spot–labyrinths	Deblauwe et al. (2008) (by inspection)
30	Mali	14.8	−3.38	Labyrinths	Leprun (1999)
31	Mali	14.94	−3.56	Labyrinths	Leprun (1999)
48	Mali	15.48	−5.83	Labyrinths	Audry and Rossetti (1962)
49	Mauritania	15.57	−5.92	Labyrinths	Audry and Rossetti (1962)
50	Mauritania	15.58	−13	Gaps	De Wispelaere (1980)
51	Nigeria	12.58	3.75	Labyrinths	Barbier et al. (2006)
52	Niger	12.7	2.63	Labyrinths	Barbier et al. (2006)
53	Niger	12.54	2.26	Gaps	Barbier et al. (2006)
54	Niger	13.12	2.17	Labyrinths	Barbier et al. (2006)
55	Sudan	11.07	27.93	Gaps	Mander et al. (2017)
56	Sudan	11.28	27.96	Gaps	Mander et al. (2017)
57	Sudan	11.27	27.55	Spots	Mander et al. (2017)
58	Sudan	11.47	27.97	Spots	Mander et al. (2017)
59	Sudan	11.51	27.87	Spots	Mander et al. (2017)
60	Sudan	11.22	27.73	Spots	Mander et al. (2017)
61	Sudan	11.62	27.86	Spots	Mander et al. (2017)
62	Sudan	11.32	27.88	Spots	Mander et al. (2017)
63	Sudan	11.37	27.68	Spots	Mander et al. (2017)
64	Sudan	11.6	27.73	Spots	Mander et al. (2017)
65	Sudan	11.46	27.68	Spots	Mander et al. (2017)
66	Sudan	11.71	27.91	Spots	Mander et al. (2017)

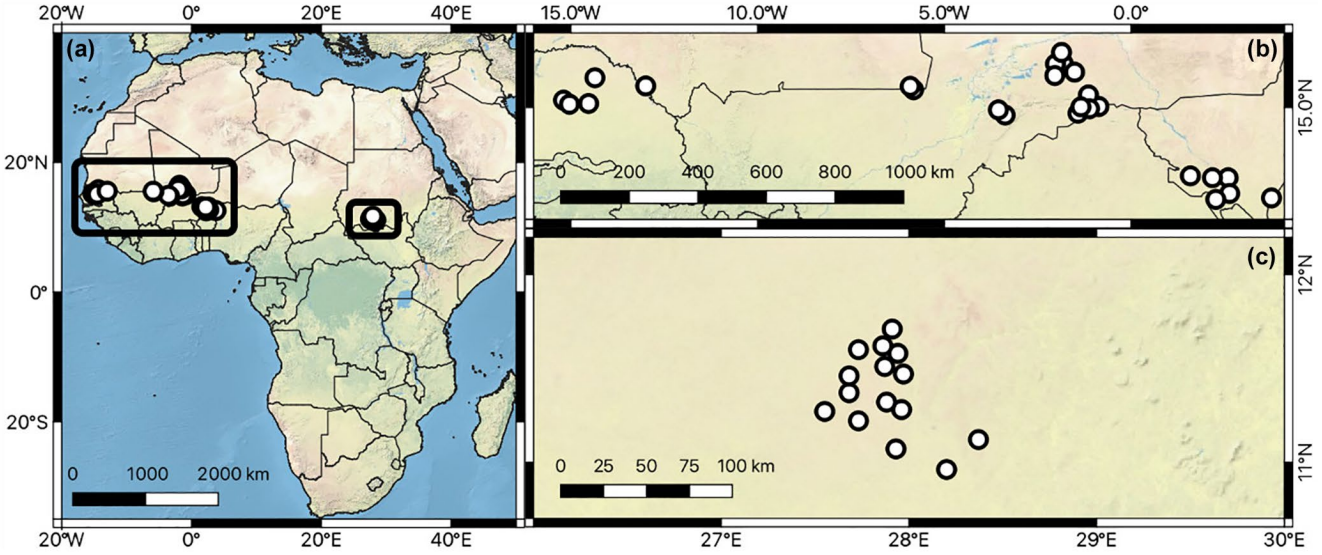

FIGURE 2 Map of patterned vegetation sites within the Sahel in North Africa. Western sites are shown in panel (b) and eastern sites are in panel (c)

where V is the number of vertices of the graph G, and E is the number of edges. This Euler characteristic is plotted for each subregion of an image to create a 20-dimensional feature vector which describes the morphology of a pattern vegetation image.

To generate a single value corresponding to a pattern's morphology, we subtract the feature vector value at the 50% point from the 100% point of the feature vector. This was chosen as this part of the vector is often more linear than the slope at the start of the vector, and allows us to convert from a vector to a scalar value. We call this value the 'Offset50'. Each sub-image has an Offset50 value, these are then averaged to form one Offset50 value per image. This process is then repeated across the full extent of the available satellite data to create an Offset50 time series.

Steps are taken at several stages of this process to ensure high-quality data and to mitigate the effects of cloud cover on Offset50 values. The formation of monthly median images removes some influence of cloud cover and aerosols. Cloud masking is applied to Sentinel 2 images in GEE; pixels which are masked will appear as completely black pixels. When the images are separated into sub-images, any sub-image which appears as completely black, due to clouds or unsuitable vegetation morphology, or completely white, such as bare soil, is rejected. For each sub-image within a given month that is rejected, we resample this by taking the mean of the same sub-image in the same month in other years. Despite this step, some interference due to cloud cover is still possible and small clouds can still be present in final images and sub-images which can lead to spurious NDVI or Offset50 values. Any values which are more than three standard deviations away from the time series mean are classed as outliers and are removed.

In images which consisted of small amounts of patterned vegetation or of mixed land cover, such as patterned vegetation and seasonal agriculture, we tested methods to remove the influence of non-patterned vegetation. These methods include reduced image sizes and image classifiers and are detailed further in the Supplementary Information (Figures S1 and S2). However, we found that these steps did little to change the trend of the results.

2.3 | Weather data

Daily precipitation data are taken from the ERA5 dataset via Google Earth Engine, which is a comprehensive reanalysis that provides hourly estimates of a large number of atmospheric, land and oceanic climate variables. Currently, ERA5 data are available from 1979 to within 5 days of real time (Hersbach et al., 2020). The dataset has a resolution of 31 km and is formed by combining as many historical observations as possible with an atmospheric model that is coupled with a land surface model and a wave model (Hersbach et al., 2020). We generate monthly averages of the ERA5 precipitation data obtained from GEE to compare with monthly NDVI and Offset50 values by plotting precipitation time series against the Offset50 time series (Figure 7) and the mean annual precipitation values at different sites. Precipitation data from 1986 to 2016 are also included in this analysis to understand the role that historical precipitation has played in the formation and stability of patterns. Furthermore, we calculate the cross-correlation of Offset50 and precipitation at increasing time lags.

2.4 | Resilience: Decay rate analysis

One way to calculate the resilience of these patterned vegetation systems is to consider rainfall as a perturbation event from a background dry state. Return rate following a perturbation can be taken

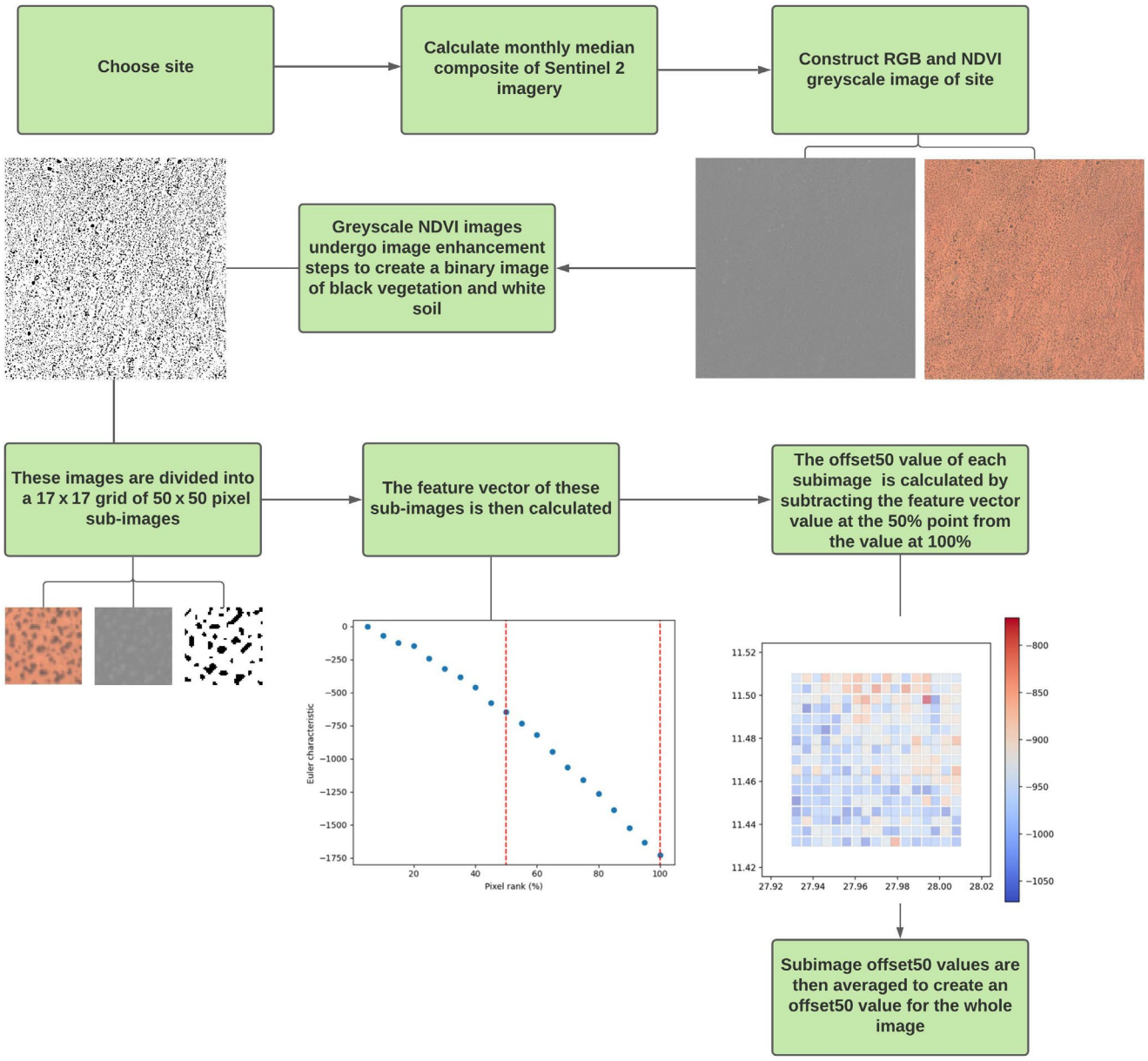

FIGURE 3 Data analysis workflow. This flow diagram shows the steps taken to calculate the Offset50 value of a patterned vegetation site (ID: 58)

as a direct measure of resilience (Lees et al., 2020; Pimm, 1984), with higher decay rates associated with more resilient systems. Usually this approach considers detrimental perturbations, instead we consider how vegetation responds to the beneficial perturbation of rainfall, yet we retain the definition that faster recovery to the background dry state equates to greater resilience (see Section 4). The average annual cycle of Offset50 and NDVI was taken with a monthly resolution. To fit an exponential model to these time series, the natural log of the average annual cycle is taken, followed by a linear regression, an example is shown in Figure 4. This was used to determine the rate of decay for the system from its peak greenness, for NDVI, or peak connectedness, for Offset50, to the state of minimum vegetation in the dry season.

2.5 | Resilience: Autocorrelation and variance

Another way to test the resilience of patterned vegetation is to calculate the well-established resilience metrics Lag-1 autocorrelation (AR(1)) and variance of Offset50 and NDVI. Prior to this, we remove the seasonality of the Offset50 and NDVI time series by calculating a multi-annual monthly average, this is then subtracted from the time series. These residuals are then smoothed by applying LOESS smoothing.

Usually when calculating AR(1), we would use a moving window of length equal to half of the time series (Boulton et al., 2014). However, due to the shortness of these time series (48 data points), the average AR(1) and variance of the whole time series were

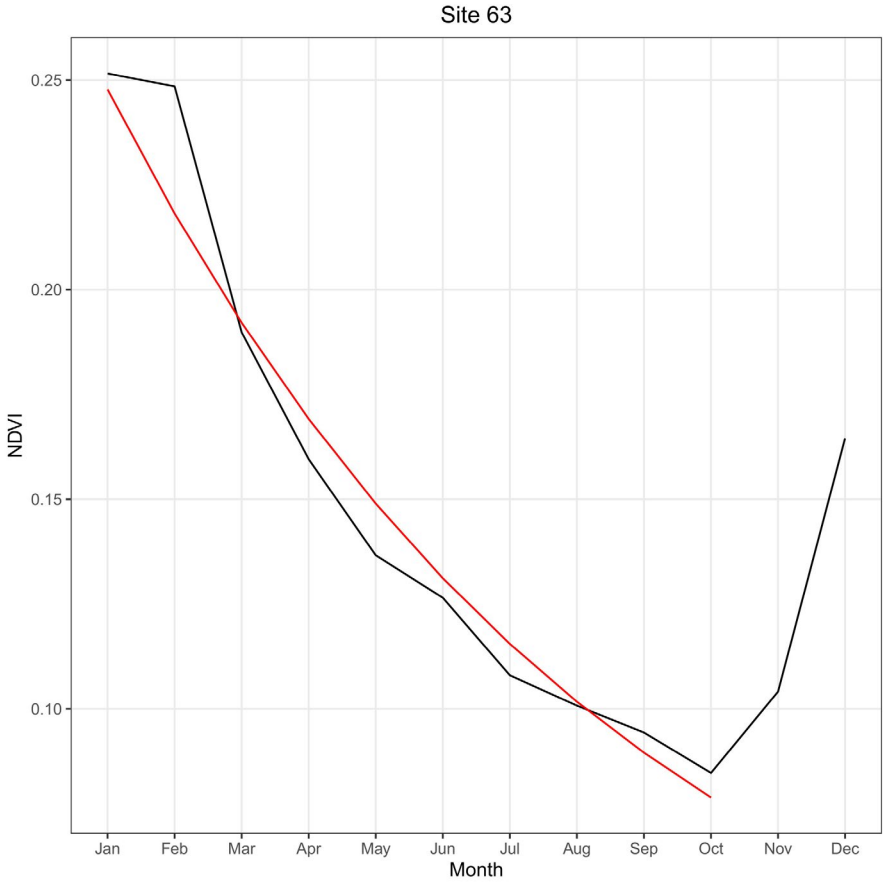

FIGURE 4 Example of exponential decay curve (red line) fitting for annual average NDVI cycle (black line) at site 63

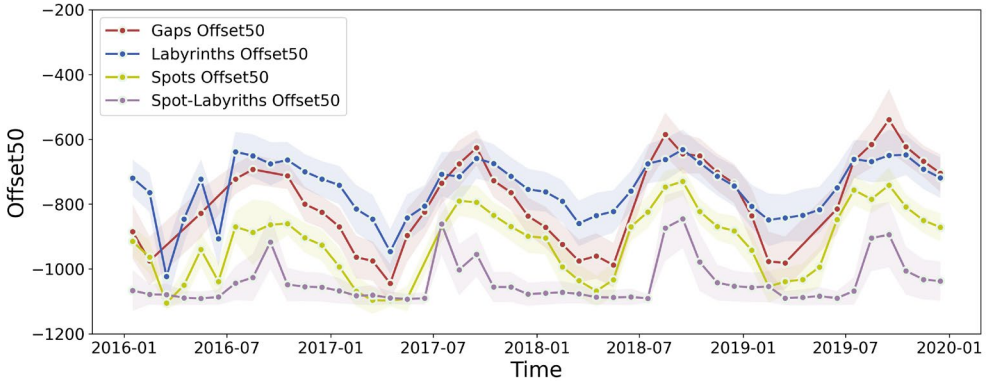

FIGURE 5 Examples of time series of Offset50 metric across four sites. An example is provided for each type of pattern. These sites correspond to the pattern type examples given in Figure 1. Offset50 standard deviation is given for each time series as the shaded area

calculated. This provides us with a single AR(1) and variance value for each time series.

2.6 | Trend analysis

STL decomposition of NDVI and Offset50 time series is used to establish the trends for each site. This separates these time series into the corresponding trend and seasonality of the underlying data. We then calculate the Mann-Kendall Tau value of this trend component. This gives a positive value if a trend is increasing, a negative value if a trend is decreasing and we classify non-significant changes as 'no trend'. We also calculate the precipitation trend of each site in this way. In addition to this, we calculate the change in precipitation in every pixel across the whole of the Sahel. This is done by taking monthly precipitation averages, removing the seasonal trend by subtracting a multi-annual monthly average, then taking a 12-month moving average, before the Kendall Tau of each pixel is calculated.

3 | RESULTS

3.1 | Distinguishing patterns with 'Offset50'

As seen in Figure 5, the Offset50 value of a site displays a seasonal cycle and tracks the changes in vegetation connectivity. The Offset50 value is different for each pattern type; for the examples shown, spot–labyrinths display the lowest Offset50 values, followed by spots, while the most connected vegetation patterns, gaps or labyrinths, display the highest Ofset50 values.

We have chosen to compare the Max NDVI and Max Offset50 values of the vegetation as this represents the extent of the vegetation following a precipitation event when the vegetation is at its full extent, is most connected, and most representative of the pattern label assigned at the classification stage (as detailed in the *Methods* section). When comparing the Max Offset50 value as grouped by vegetation pattern (Figure 6), we can see that they are broadly distinct classes; there is some overlap between gaps and labyrinths, although gaps display broadly larger values. We also find that despite the visual similarities between 'spot–labyrinths' and conventional labyrinths and spots, they exist as a distinct class. Max NDVI values for each pattern type are also given. U-tests suggest that the max Offset50 of each pattern for these sample sites is statistically significantly different to each other ($p < .05$; Table S2). When using U-tests to distinguish between the pattern classes for Max NDVI values, we find that while the gaps vegetation is distinct, the rest of the vegetation classes are not statistically significantly distinct (Table S3). When compared with the Max NDVI of a site over the same time period, we can see that Max Offset50 does a better job of differentiating between the different patterns.

3.2 | Seasonal and interannual variability of Offset50

As can be seen in Figure 7, the timing of the peak of Offset50 is closely linked with the peak of the annual precipitation cycle, with this peak occurring either within the same or following month of the precipitation peak. The Offset50 signal then decays away following the end of the rainy season. At the peak Offset50 value '(a)' in Figure 7, there is much more vegetation cover than during the dry season '(b)'.

The vegetation shown in Figure 8 is classified as 'spot–labyrinths'. This vegetation forms a pattern which resembles faint, degraded spots in drier years, while in wetter periods it forms interlinked stripes across the landscape. The morphology of these patterns appears to be topographically driven, with vegetation forming within shallow gullies and between sand dunes following a rainy season. These patterns display strong interannual variability. It is clear that if there is not sufficient rain within a season, then much of the vegetation will not grow.

3.3 | Factors determining Offset50 and vegetation pattern resilience

Figure 9 displays the correlation values for important variables which measure vegetation connectedness (Offset50), abiotic influences (precipitation, latitude) and measures of resilience of vegetation (decay rates, AR(1), variance). We have used these to further understand the dynamics and resilience of the vegetation pattern system as well as the utility of our Offset50 metric.

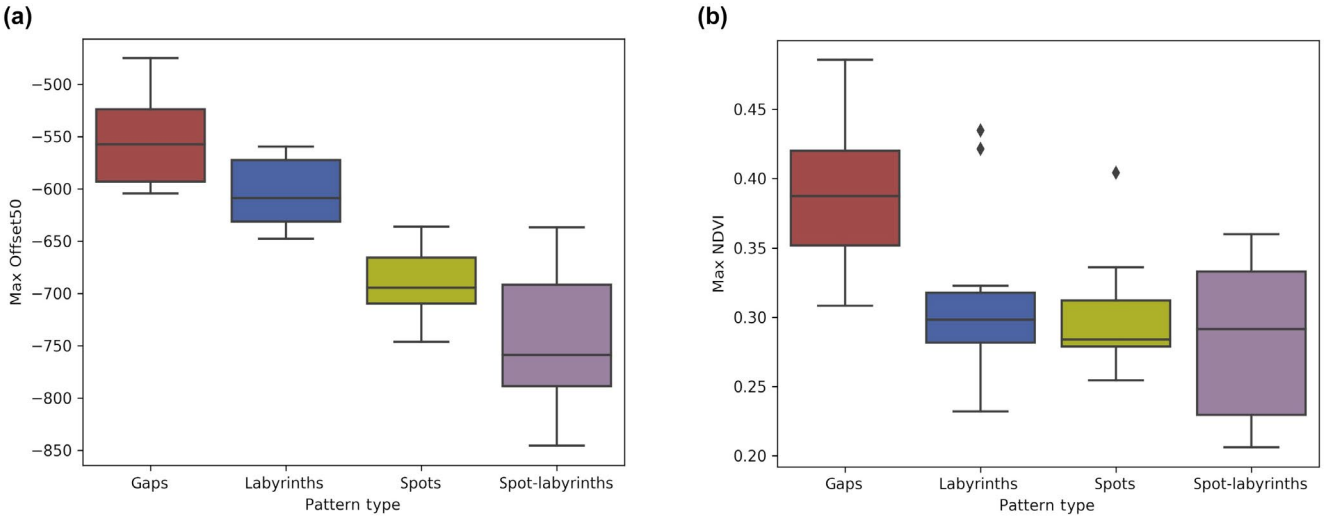

FIGURE 6 (a) Box plots of Max Offset50 values for pattern vegetation sites as grouped by pattern classification. Two tailed Mann–Whitney U-tests suggest that the Max Offset50 value for these group classes are statistically significantly different from each other (*p*-values in Table S2). (b) Box plots of Max NDVI values for pattern vegetation sites as grouped by pattern classification. Use of a Mann–Whitney U-test suggests that while the gaps class may be distinct from the other groups, there is no statistically significant difference between the other classes (Table S3). Mean Offset50 and Mean NDVI are shown in Figure S5

3.3.1 | Precipitation and Offset50

As seen in Figure 9, Offset50 max displays a significant moderate positive correlation with mean precipitation, while Offset50 mean has a strong positive correlation with precipitation. This means that 'gap' sites are the wettest, while 'spot–labyrinth' sites are the driest. Thus, precipitation levels contribute to pattern morphology, as measured by Offset50.

The historic precipitation mean from 1976 to 2016 is included to understand whether historic climate has influenced the current pattern morphology or its resilience. We find that while historic rainfall means do correlate with the Offset50 metric, these correlations are less strong than current precipitation levels, noting also the strong link between historical and current precipitation levels.

As can be seen in Figure 10, there is a lagged relationship between precipitation and the Offset50 metric across all of the sites. With a close coupling between precipitation and vegetation, these sites experience one significant rainy season per year, after which the vegetation reaches its maximum extent, and therefore so does the Offset50.

There are two trends apparent in this plot, with most sites experiencing the highest correlation between Offset50 and precipitation after 1 month. A clustering analysis of these trends reveals that there are two separate groupings (as seen in Figure S14), with one group composed almost entirely of all of the spot–labyrinth sites. These sites display a faster decline in the correlation between Offset50 and precipitation following their initial peak. We propose that this is due to the morphological nature of these patterns, in addition to needing to have a certain threshold of rainfall to enable large-scale vegetation growth.

3.3.2 | Resilience

As seen in Figure 9, the Offset50 decay rate has a significant moderately positive correlation with the average precipitation. Therefore, areas with higher rainfall are (by convention) more 'resilient' following this perturbation. This is perhaps a surprising result, as it suggests that areas with a higher level of precipitation experience a faster decay from the peak vegetation state to the minimum vegetation state and that this base state is more resilient. Importantly, Offset50 decay rate does not show a significant correlation to either maximum or mean Offset50 values, thus suggesting that pattern morphology does not correlate with a decay rate measure of resilience (and this null result would, of course, still hold if we inverted our assumed relationship between decay rate and resilience).

When we consider the NDVI decay rate (Table S6), we find it is greater at wetter sites. We also find a strong positive correlation between average NDVI and NDVI decay rate. Therefore, wetter sites with higher NDVI levels have a higher decay rate from maximum greenness to the bare soil state.

For our other metrics of resilience of vegetation patterns, AR(1) and variance of Offset50, there are significant, moderate negative correlations with mean precipitation (Figure 9). Thus, wetter sites have a higher level of resilience of vegetation patterns by these metrics. However, we find that there is no significant correlation between mean or max Offset50 and AR(1) or variance of Offset50. This fails to support the hypothesis from the literature that the morphology of a pattern affects its resilience.

There are also significant weak positive correlations between AR(1) or variance of Offset50 and latitude. This supports an observation in the literature that more northern sites are less resilient (Trichon et al., 2018). This is likely driven by the lower level of precipitation at higher latitudes.

There is a weak negative correlation (which tends towards significance, $p < .1$) between AR(1) or variance and longitude (Figure 9)—that is, resilience increases with longitude. This is likely linked to a strong positive correlation between longitude and precipitation (Figure 9).

3.4 | Offset50 and precipitation trends across sites

We now turn to trends in the absolute values of precipitation and Offset50 across sites (Figure 11).

Western sites, such as those in Senegal, display a negative trend of Offset50, while those in Mali are much more mixed. Eastern sites all show a positive or no Offset50 trend. Sites with positive Offset50 trends are broadly clustered in areas with a positive precipitation trend, while negative Offset50 trends are clustered in areas where there has been a declining level of precipitation from 2016 to 2019. This makes sense given the established positive correlation between Offset50 and rainfall (Figure 9).

4 | DISCUSSION

4.1 | Utility of Offset50 metric and relationship with precipitation

This study provides a framework for vegetation pattern quantification and long-term analysis of these sites within the Sahel. The *pyveg* package (Barlow et al., 2020) allows for long-term analysis of patterned vegetation sites, which often occur in hard to reach places around the world. By building on the work presented in Mander et al. (2017), we use Offset50, a numerical metric, to quantify vegetation patterns using freely available satellite data. Previous studies have sought to visually assess vegetation pattern health using infrequent aerial photography (Couteron, 2002; Trichon et al., 2018), these are often limited in extent both spatially and temporally. Sentinel-2 data, with its 10 m resolution, when combined with the *pyveg* package, provide a way to repeatedly analyse pattern vegetation anywhere in the world and to generate time series of its state. We find that our Offset50 metric is more capable than NDVI of differentiating

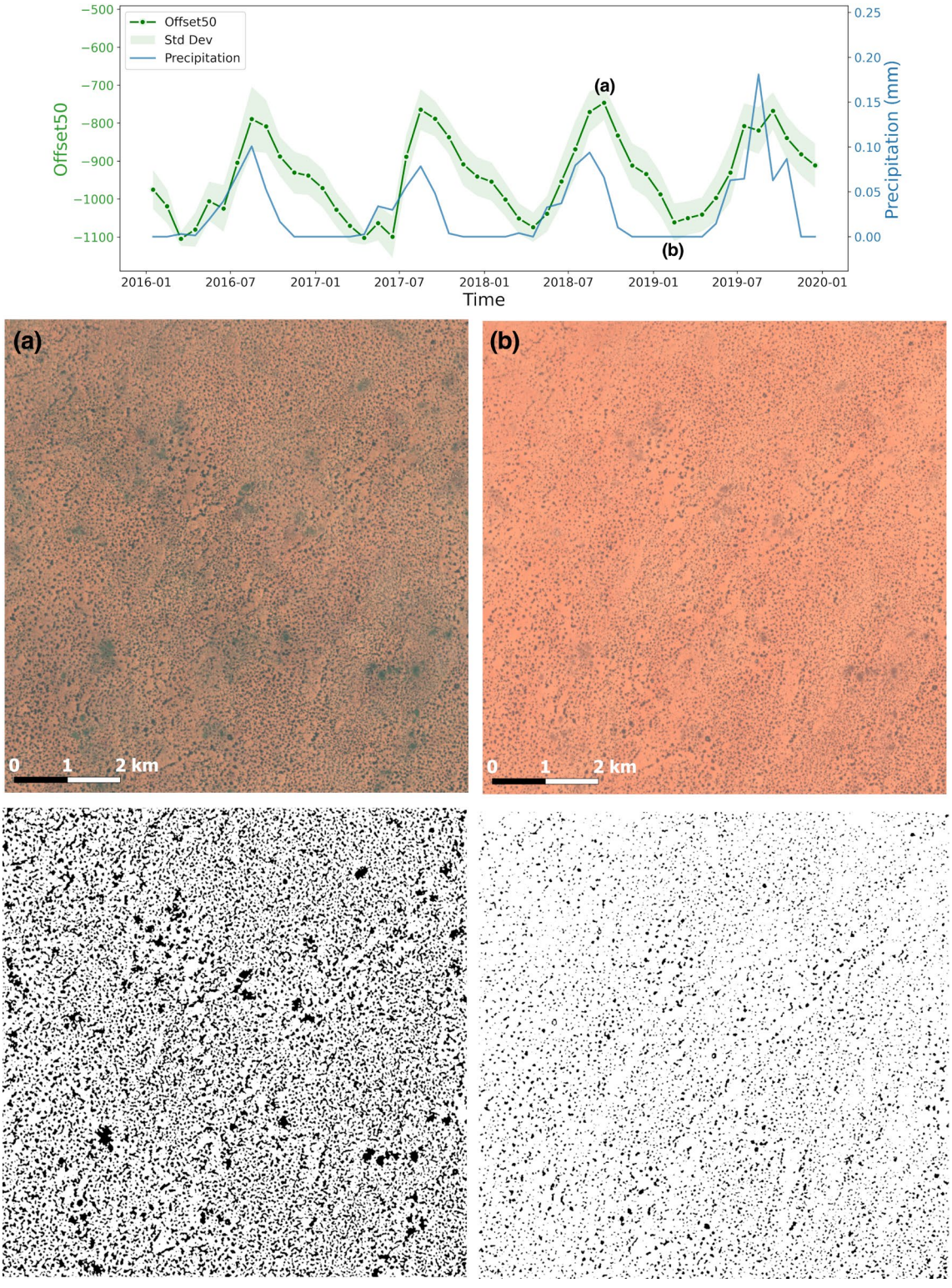

FIGURE 7 Example of Offset50 seasonal variability in a spotted vegetation site (ID: 61) with (a) an image of the vegetation at its 2018 peak and (b) the following Offset50 minimum in March 2019. Shown below (a) and (b) are the binary images used to calculate the Offset50 value for that month. In these binary images, black pixels are vegetation, while white pixels are bare soil

between four pattern vegetation classes at their maximum extent; gaps, labyrinths, spots and spot–labyrinths. This allows us to quantify inter- and intra-annual changes in vegetation pattern morphology.

Precipitation levels have often been identified as the predominant factor in patterned vegetation formation and morphology (HilleRisLambers et al., 2001). The correlation between

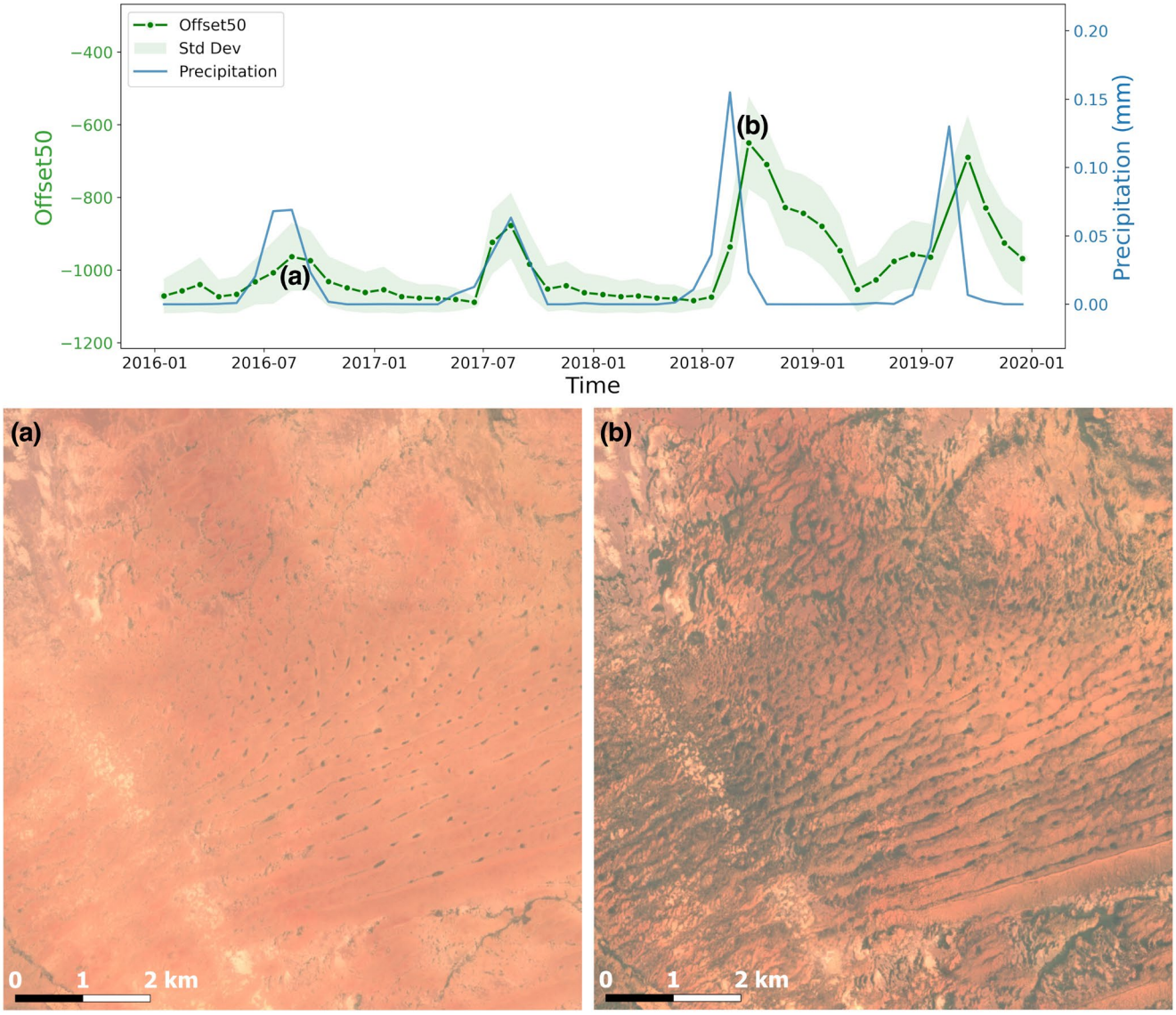

FIGURE 8 An example of interannual variability of spot–labyrinth vegetation (ID: 26). This displays the extreme variation in this vegetation with (a) an example of peak vegetation cover in a dry year and (b) an example of peak vegetation cover in a comparatively wet year. The formation of this vegetation is influenced by the topography, as detailed in Figure S3

Offset50 values and average precipitation levels at our sites shows that our Offset50 metric successfully captures this relationship. We have also considered the lagged correlation between Offset50 and precipitation, which for most sites peaks after 1 month and then declines. The difference between spot–labyrinths and other vegetation types is clear in the lagged correlation trend. This further reveals the different mechanisms of formation of the vegetation morphologies, with the lagged correlation decreasing faster for the spot–labyrinth sites. This is likely to be the result of vegetation formation from the collection of rainfall within gullies and between sand dunes, within which the vegetation then grows. If this precipitation stays below a certain threshold, then the vegetation is minimal and unconnected.

4.2 | Resilience

We have taken two different approaches to measuring the resilience of vegetation patterns by examining different time-series properties of the Offset50 metric.

First we considered the decay rate of Offset50 following the annual rainy season. The conventional understanding is that a faster decay rate equates to a more resilient system. Following this convention, we find that sites which have higher precipitation display a higher decay rate and are therefore more 'resilient'. However, this is somewhat counter-intuitive, in that it refers to the resilience of the dry season minimum vegetation cover state, which is found to be more 'resilient' under higher precipitation levels. We also find the same result when considering the NDVI decay rate. This suggests

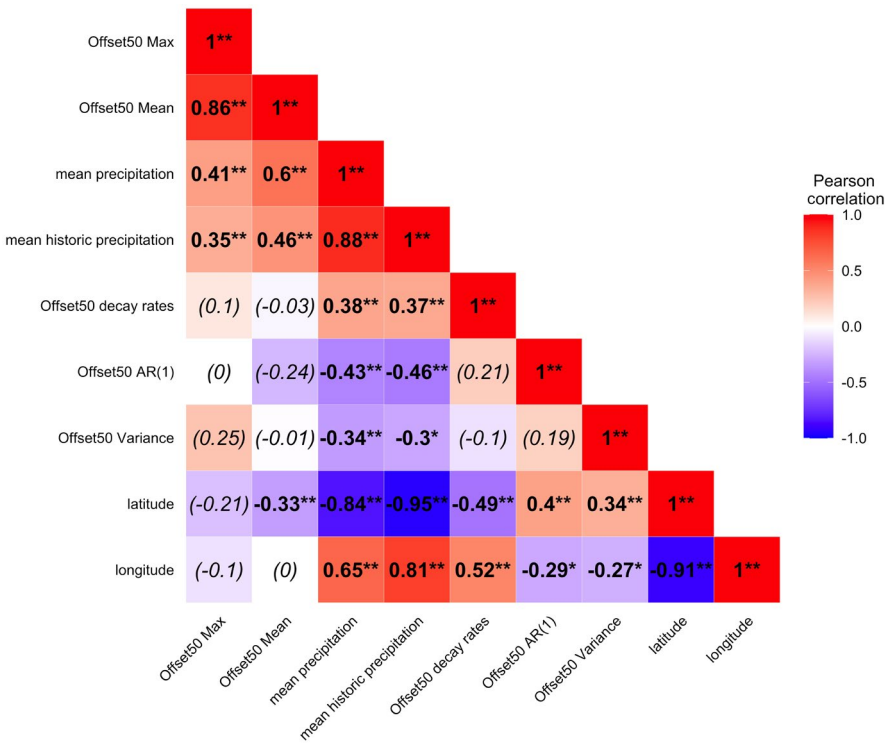

FIGURE 9 Correlation image showing Pearson's correlation values for Offset50 precipitation correlation, Offset50 decay rate correlations and AR(1) and Variance correlations. Values in bold are significant, with ** corresponding to $p < .05$ and * corresponding to $p < .1$. Scatter plots are given in Figures S6–S13. Pearson's correlation coefficient and p-values for Offset50 and NDVI variables are given in Tables S4–S7

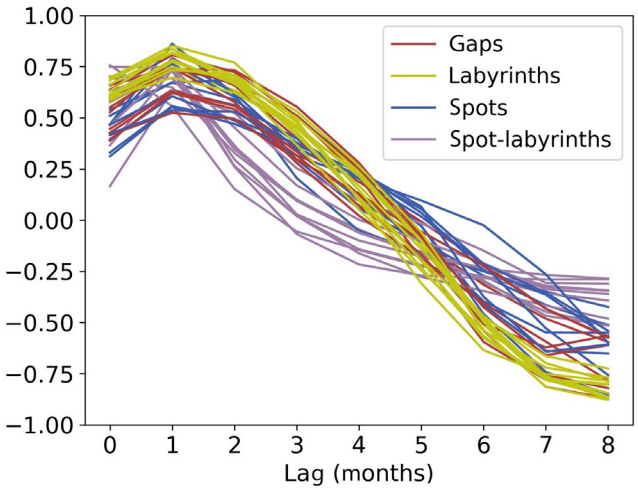

FIGURE 10 Correlation between Offset50 and precipitation at increasing monthly lags across all sites. Each line represents one of the sites in this study

that, while higher levels of precipitation may lead to a larger burst in vegetation cover, it tends to die off faster. This can also be seen in the positive correlation between average precipitation and NDVI standard deviation (correlation = 0.4752, $p = .0019$), with wetter sites showing greater standard deviation due to the greater quantity of vegetation die off each year.

Second we removed the seasonal cycle and then calculated Lag-1 autocorrelation (AR(1)) and variance of the detrended Offset50 time series, both of which are conventional resilience measures. This probes behaviour on shorter timescales than the annual cycle, which is appropriate given the multi-month memory in the system (Figure 10). We find that sites which experience higher precipitation levels show lower AR(1) and variance levels and are therefore more resilient according to these metrics. This is in agreement with our understanding of rainfall levels and vegetation morphology, and suggests that vegetation which exists under lower rainfall regimes may be at risk of further degradation or state transitions. This is supported by results found in the literature, which find that drier sites have experienced greater levels of degradation during a drought period and have been less able to recover (Trichon et al., 2018). We consider the relationship between historical precipitation levels and patterned vegetation resilience to understand the effect that past climate may have had on the adaptive capacity of patterned vegetation. While there is some correlation, this is most likely due to the strong correlation between historic and modern precipitation, as opposed to any underlying property of the system.

We also tested the hypothesis that vegetation pattern morphology itself provides a measure of resilience (Mayor et al., 2013; Rietkerk et al., 2004). Dakos et al. (2011) suggest that while critical slowing down is observed as pattern morphology shifts in a 'scale-dependent feedback' vegetation model, there is no consistent increase in AR(1) with these changes. This is in line with our results, which show that pattern morphology does not significantly correlate with any of the resilience indicators we consider; decay rate, AR(1) or variance. This suggests that while the nature of vegetation patterning does reflect underlying precipitation, it cannot be linked directly to the resilience of the vegetation, at least across the sample of 40 sites we consider.

There is evidence that severe and prolonged droughts cause a greater reduction in coverage of northern Sahelian patterned

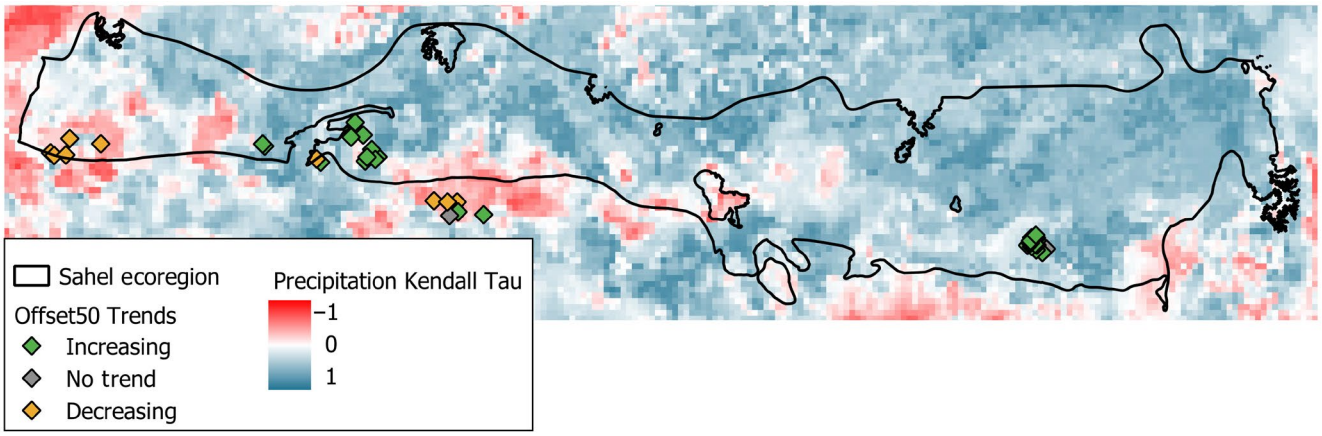

FIGURE 11 ERA5 Precipitation trends from 2016 to 2019 in the vicinity of the Sahel ecoregion. Also shown are the Offset50 trends of each patterned vegetation site. NDVI trends are given in Figures S15 and S16

vegetation sites (Trichon et al., 2018). This is consistent with our results that patterned vegetation sites at higher latitudes have a lower level of resilience, likely linked to the lower levels of precipitation at higher latitude.

4.3 | Trends in Offset50

Identification of trends in Offset50 between 2016 and 2019 in sites across the Sahel reveals a mixed picture. No sites with negative trends for Offset50 appear in the east of the Sahel, while these are more common in the west. This is in line with trends in precipitation (Figure 11), with declining Offset50 trends situated in areas with declining precipitation trends. Nicholson et al. (2018) identify a difference in rainfall between the east and west, with the eastern precipitation regime showing a greater recovery from historic dry periods. This east–west division is reinforced by the eastern vegetation sites displaying higher resilience levels. However, more data are needed to understand whether this east–west divide in patterned vegetation trends is sustained at the decadal level. A more global analysis could provide an indication of different pattern vegetation resilience and the drivers of this. Aside from climatic factors, other potential causes of declining pattern vegetation cover, and therefore declining Offset50, relate to human activities, such as the collection of forage for livestock, or the conversion of land to agriculture.

4.4 | Limitations and future work

Interference from cloud cover creates difficulties for most remote sensing studies. In this study, we have sought to limit the impact of cloud cover through numerous methods, as detailed in the *Methods*. There are some limitations introduced by the availability of satellite data. Sentinel-2 was launched in 2015; therefore, we have been unable to observe multi-decadal trends in the patterned vegetation at the appropriate scale. The time series was also determined to be too short to conduct some forms of time-series analysis. To counter this, attempts were made to use data from Landsat 7 and Landsat 8 to provide longer analysis at lower spatial resolution; however, well-documented issues with the Landsat 7 scan line error (Scaramuzza and Barsi, 2005) prevented this.

In addition to this, attempts were made to source vegetation patterning from a diverse range of sites across the Sahel. This was successful for every form apart from spots, where difficulty with establishing degraded spot sites meant the removal of several sites from the dataset. This meant that all of the sites are located within a similar area of Sudan. This was further compounded by inconsistencies in historical literature in spot definition, with gaps and spots often interchangeable terms. Some sites which were identified in historical literature as showing spotted vegetation were limited in size and difficult to analyse or have since become much more degraded.

The creation of the *pyveg* package will allow future work to continue monitoring pattern vegetation morphology and the health of dryland ecosystems. The increasing availability of high-resolution Sentinel-2 images will enable longer and more in-depth time-series analysis. In addition to this, future work could apply the *pyveg* package to global drylands to develop a more comprehensive understanding of resilience trends in these regions.

Based upon the lack of relationship between pattern morphology and resilience, we suggest that further work is required to define and measure resilience of these patterned systems. With an increased availability of sufficiently high-resolution satellite data, we believe that other resilience tools should be brought to bear on these systems, with consideration given to spatial resilience statistics as well as temporal analysis.

5 | CONCLUSION

Dryland ecosystems are among the most sensitive to climate change. Accurately assessing and understanding vegetation patterning morphology is an important step towards understanding

the effect of a changing climate and direct anthropogenic pressure on drylands. Here we have shown that a previously proposed feature vector Offset50 metric detects changes in pattern vegetation morphology and is sensitive to changes in precipitation, the underlying driver of pattern vegetation. We find that three different measures of resilience—the decay rate from perturbation, AR(1) and variance of Offset50—all show declining resilience of vegetation patterns with declining rainfall (as do the same statistics for NDVI). However, we find no significant correlation between the Offset50 pattern metric and any of these three measures of resilience. This fails to support a widely cited hypothesis in the literature that the nature of vegetation pattern (quantified here) reflects resilience. This negative result should not be wholly surprising, as we are unaware of any theoretical demonstration that there should be a direct relationship between regular pattern morphology and resilience. We also find that geographical gradients of patterned vegetation resilience reflect well-known rainfall gradients, and that recent trends in rainfall are largely reflected in corresponding trends in vegetation patterns. Notably, consistent recent wetting of eastern sites is reflected in positive trends in Offset50, while the picture for the west is more mixed. As a longer timescale sample of high-resolution satellite data accumulates, this should enable further enhanced understanding of the resilience of these special ecosystems.

ACKNOWLEDGEMENTS

This work was supported by The Leverhulme Trust (grant number: RPG-2018-046), The Alan Turing Institute under the Turing Fellowship (grant number: R-EXE-001) and the UCL CDT in Data Intensive Science (grant number: ST/P006736/1).

AUTHOR CONTRIBUTIONS

JB contributed to study conceptualization, undertaking the study, providing materials and/or scripts, analysing and interpreting the data, writing and editing the manuscript. JA contributed to study conceptualization, undertaking the study, analysing and interpreting the data, writing and editing the manuscript. CB contributed to study conceptualization, analysing and interpreting the data, editing the manuscript. NB contributed to undertaking the study, providing materials and/or scripts, editing the manuscript. CRS contributed to undertaking the study, providing materials and/or scripts, editing the manuscript. SVS contributed by providing materials and/or scripts, editing the manuscript. KL contributed to study conceptualization, analysing and interpreting the data, editing the manuscript. TL contributed to study conceptualization, analysing and interpreting the data, writing and editing the manuscript.

DATA AVAILABILITY STATEMENT

The data that support the findings of this study are openly available in Zenodo. Processed images can be found at https://doi.org/10.5281/zenodo.5536861. Analysis results can be found at https://doi.org/10.5281/zenodo.4050362.

ORCID

Joshua E. Buxton https://orcid.org/0000-0001-9664-0368
Jesse F. Abrams https://orcid.org/0000-0003-0411-8519
Chris A. Boulton https://orcid.org/0000-0001-7836-9391
Nick Barlow https://orcid.org/0000-0003-3284-5342
Camila Rangel Smith https://orcid.org/0000-0002-0227-836X
Samuel Van Stroud https://orcid.org/0000-0002-7969-0301
Kirsten J. Lees https://orcid.org/0000-0001-9254-2103
Timothy M. Lenton https://orcid.org/0000-0002-6725-7498

REFERENCES

Audry, P., & Rossetti, C. (1962). Observations sur les sols et la végétation en Mauritanie du sud-est et sur la bordure adjacente du Mali (1959 et 1961).

Barbier, N., Couteron, P., Lejoly, J., Deblauwe, V., & Lejeune, O. (2006). Self-organized vegetation patterning as a fingerprint of climate and human impact on semi-arid ecosystems. *Journal of Ecology*, *94*(3), 537–547.

Barlow, N., Rangel Smith, C., Van Stroud, S., Abrams, J., Boulton, C., & Buxton, J. (2020). pyveg: A Python package for analysing the time evolution of patterned vegetation using google earth engine. *Journal of Open Source Software*, *5*(55), 2483. https://doi.org/10.21105/joss.02483

Beegle, K., & Christiaensen, L. (2019). *Accelerating Poverty Reduction in Africa*. World Bank. © World Bank. https://openknowledge.worldbank.org/handle/10986/32354. License: CC BY 3.0 IGO.

Boulton, C. A., Allison, L. C., & Lenton, T. M. (2014). Early warning signals of Atlantic meridional overturning circulation collapse in a fully coupled climate model. *Nature Communications*, *5*(1), 1–9. https://doi.org/10.1038/ncomms6752

Charney, J. G. (1975). Dynamics of deserts and drought in the Sahel. *Quarterly Journal of the Royal Meteorological Society*, *101*(428), 193–202. https://doi.org/10.1002/qj.49710142802

Chen, Y., Kolokolnikov, T., Tzou, J., & Gai, C. (2015). Patterned vegetation, tipping points, and the rate of climate change. *European Journal of Applied Mathematics*, *26*(06), 945–958. https://doi.org/10.1017/S0956792515000261

Couteron, P. (2002). Quantifying change in patterned semi-arid vegetation by Fourier analysis of digitized aerial photographs. *International Journal of Remote Sensing*, *23*(17), 3407–3425. https://doi.org/10.1080/01431160110107699

Dai, L., Korolev, K. S., & Gore, J. (2013). Slower recovery in space before collapse of connected populations. *Nature*, *496*(7445), 355–358. https://doi.org/10.1038/nature12071

Dakos, V., Kéfi, S., Rietkerk, M., Van Nes, E. H., & Scheffer, M. (2011). Slowing down in spatially patterned ecosystems at the brink of collapse. *The American Naturalist*, *177*(6), E153–E166. https://doi.org/10.1086/659945

Dakos, V., Scheffer, M., van Nes, E. H., Brovkin, V., Petoukhov, V., & Held, H. (2008). Slowing down as an early warning signal for abrupt climate change. *Proceedings of the National Academy of Sciences*, *105*(38), 14308–14312. https://doi.org/10.1073/pnas.0802430105

De Wispelaere, G. (1980). Les photographies aériennes témoins de la dégradation du couvert ligneux dans un géosystème sahélien sénégalais. *Cahiers ORSTOM Série Sciences Humaines*, *27*(3–4), 155–166.

Deblauwe, V., Barbier, N., Couteron, P., Lejeune, O., & Bogaert, J. (2008). The global biogeography of semi-arid periodic vegetation patterns. *Global Ecology and Biogeography*, *17*(6), 715–723. https://doi.org/10.1111/j.1466-8238.2008.00413.x

Doso, S., Jr. (2014). Land degradation and agriculture in the Sahel of Africa: Causes, impacts and recommendations. *Journal of*

Agricultural Science and Applications, *3*(03), 67–73. https://doi.org/10.14511/jasa.2014.030303

Drusch, M., Del Bello, U., Carlier, S., Colin, O., Fernandez, V., Gascon, F., Hoersch, B., Isola, C., Laberinti, P., Martimort, P., Meygret, A., Spoto, F., Sy, O., Marchese, F., & Bargellini, P. (2012). Sentinel-2: ESA's optical high-resolution mission for GMES operational services. *Remote Sensing of Environment*, *120*, 25–36. https://doi.org/10.1016/j.rse.2011.11.026

Estrada, E., & Rodriguez-Velazquez, J. A. (2005). Subgraph centrality in complex networks. *Physical Review E*, *71*(5), 56103. https://doi.org/10.1103/PhysRevE.71.056103

Gorelick, N., Hancher, M., Dixon, M., Ilyushchenko, S., Thau, D., & Moore, R. (2017). Google earth engine: Planetary-scale geospatial analysis for everyone. *Remote Sensing of Environment*, *202*, 18–27. https://doi.org/10.1016/j.rse.2017.06.031

Gowda, K., Iams, S., & Silber, M. (2018). Signatures of human impact on self-organized vegetation in the Horn of Africa. *Scientific Reports*, *8*, 3622. https://doi.org/10.1038/s41598-018-22075-5

Helldén, U. (1991). Desertification: Time for an assessment? *Ambio*, *20*(8), 372–383.

Hermann, S. M., & Hutchinson, C. F. (2005). The changing contexts of the desertification debate. *Journal of Arid Environments*, *63*(3), 538–555. https://doi.org/10.1016/j.jaridenv.2005.03.003

Hersbach, H., Bell, B., Berrisford, P., Hirahara, S., Horányi, A., Muñoz-Sabater, J., Nicolas, J., Peubey, C., Radu, R., Schepers, D., Simmons, A., Soci, C., Abdalla, S., Abellan, X., Balsamo, G., Bechtold, P., Biavati, G., Bidlot, J., Bonavita, M., … Thépaut, J.-N. (2020). The ERA5 global reanalysis. *Quarterly Journal of the Royal Meteorological Society*, *146*(730), 1999–2049. https://doi.org/10.1002/qj.3803

HilleRisLambers, R., Rietkerk, M., van den Bosch, F., Prins, H. H., & de Kroon, H. (2001). Vegetation pattern formation in semi-arid grazing systems. *Ecology*, *82*(1), 50–61. https://doi.org/10.1890/0012-9658(2001)082[0050:VPFISA]2.0.CO;2

IPBES. (2018). The IPBES assessment report on land degradation and restoration. In L. Montanarella, R. Scholes, & A. Brainich (Eds.), *Secretariat of the intergovernmental science-policy platform on biodiversity and ecosystem services* (p. 744). https://doi.org/10.5281/zenodo.3237392

Kéfi, S., Guttal, V., Brock, W. A., Carpenter, S. R., Ellison, A. M., Livina, V. N., Seekell, D. A., Scheffer, M., van Nes, E. H., & Dakos, V. (2014). Early warning signals of ecological transitions: methods for spatial patterns. *PLoS One*, *9*(3), e92097. https://doi.org/10.1371/journal.pone.0092097

Konings, A. G., Dekker, S. C., Rietkerk, M., & Katul, G. G. (2011). Drought sensitivity of patterned vegetation determined by rainfall-land surface feedbacks. *Journal of Geophysical Research: Biogeosciences*, *116*, G04008. https://doi.org/10.1029/2011JG001748

Kusserow, H. (2017). Desertification, resilience, and re-greening in the African Sahel–a matter of the observation period? *Earth System Dynamics*, *8*(4), 1141. https://doi.org/10.5194/esd-8-1141-2017

Le Houérou, H. N. (1989). *The grazing land ecosystems of the African Sahel*. Ecological Studies *75* (p. 282). Springer.

Leblanc, M. J., Favreau, G., Massuel, S., Tweed, S. O., Loireau, M., & Cappelaere, B. (2008). Land clearance and hydrological change in the Sahel: SW Niger. *Global and Planetary Change*, *61*(3–4), 135–150. https://doi.org/10.1016/j.gloplacha.2007.08.011

Lees, K. J., Artz, R. R. E., Chandler, D., Aspinall, T., Boulton, C. A., Buxton, J., Cowie, N. R., & Lenton, T. M. (2020). Using remote sensing to assess peatland resilience by estimating soil surface moisture and drought recovery. *Science of The Total Environment*, *761*, 143312.

Lenton, T. M. (2011). Early warning of climate tipping points. *Nature Climate Change*, *1*(4), 201–209. https://doi.org/10.1038/nclimate1143

Leprun, J. C. (1999). The influences of ecological factors on tiger bush and dotted bush patterns along a gradient from Mali to northern Burkina Faso. *Catena*, *37*(1–2), 25–44. https://doi.org/10.1016/S0341-8162(98)00054-X

Mander, L., Dekker, S. C., Li, M., Mio, W., Punyasena, S. W., & Lenton, T. M. (2017). A morphometric analysis of vegetation patterns in dryland ecosystems. *Royal Society Open Science*, *4*(2), 160443. https://doi.org/10.1098/rsos.160443

May, J. F., Guengant, J. P., & Barras, V. (2017). Demographic challenges of the Sahel countries. In: *Africa's population. In search of a demographic dividend* (pp. 165–177). Springer.

Mayor, A. G., Kéfi, S., Bautista, S., Rodríguez, F., Cartení, F., & Rietkerk, M. (2013). Feedbacks between vegetation pattern and resource loss dramatically decrease ecosystem resilience and restoration potential in a simple dryland model. *Landscape Ecology*, *28*(5), 931–942. https://doi.org/10.1007/s10980-013-9870-4

Meron, E., Gilad, E., von Hardenberg, J., Shachak, M., & Zarmi, Y. (2004). Vegetation patterns along a rainfall gradient. *Chaos, Solitons & Fractals*, *19*(2), 367–376. https://doi.org/10.1016/S0960-0779(03)00049-3

Nicholson, S. E., Fink, A. H., & Funk, C. (2018). Assessing recovery and change in West Africa's rainfall regime from a 161-year record. *International Journal of Climatology*, *38*(10), 3770–3786. https://doi.org/10.1002/joc.5530

Nicholson, S. E., Tucker, C. J., & Ba, M. B. (1998). Desertification, drought, and surface vegetation: An example from the West African Sahel. *Bulletin of the American Meteorological Society*, *79*(5), 815–830. https://doi.org/10.1175/1520-0477(1998)079<0815:DDASVA>2.0.CO;2

Penny, G. G., Daniels, K. E., & Thompson, S. E. (2013). Local properties of patterned vegetation: quantifying endogenous and exogenous effects. *Philosophical Transactions of the Royal Society A: Mathematical, Physical and Engineering Sciences*, *371*(2004), 20120359.

Pimm, S. L. (1984). The complexity and stability of ecosystems. *Nature*, *307*(5949), 321–326. https://doi.org/10.1038/307321a0

Raleigh, C. (2010). Political marginalization, climate change, and conflict in African Sahel states. *International Studies Review*, *12*(1), 69–86. https://doi.org/10.1111/j.1468-2486.2009.00913.x

Rietkerk, M., Dekker, S., de Ruiter, P., & van de Koppel, J. (2004). Self-organized patchiness and catastrophic shifts in ecosystems. *Science*, *305*, 1926–1929

Rouse, J. W., Haas, R. H., Scheel, J. A., & Deering, D. W. (1974) Monitoring vegetation systems in the great plains with ERTS. Proceedings, 3rd Earth Resource Technology Satellite (ERTS) Symposium (vol. *1*, pp. 48-62).

Sanchez, P. A. (2002). Soil fertility and hunger in Africa. *Science*, *295*(5562), 2019–2020. https://doi.org/10.1126/science.1065256

Scaramuzza, P., & Barsi, J. (2005). Landsat 7 scan line corrector-off gap-filled product development. In: *Proceeding of Pecora* (vol. *16*, pp. 23–27).

Scheffer, M., Bascompte, J., Brock, W. A., Brovkin, V., Carpenter, S. R., Dakos, V., Held, H., van Nes, E. H., Rietkerk, M., & Sugihara, G. (2009). Early-warning signals for critical transitions. *Nature*, *461*(7260), 53–59. https://doi.org/10.1038/nature08227

Scheffer, M., Carpenter, S., Foley, J. A., Folke, C., & Walker, B. (2001). Catastrophic shifts in ecosystems. *Nature*, *413*(6856), 591–596. https://doi.org/10.1038/35098000

Siero, E., Siteur, K., Doelman, A., Koppel, J. V. D., Rietkerk, M., & Eppinga, M. B. (2019). Grazing away the resilience of patterned ecosystems. *The American Naturalist*, *193*(3), 472–480. https://doi.org/10.1086/701669

Trichon, V., Hiernaux, P., Walcker, R., & Mougin, E. (2018). The persistent decline of patterned woody vegetation: The tiger bush in the context of the regional Sahel greening trend. *Global Change Biology*, *24*(6), 2633–2648. https://doi.org/10.1111/gcb.14059

Turing, A. (1952). The Chemical basis of morphogenesis. *Philosophical Transactions of the Royal Society B*, *237*, 37.

Valentin, C., & d'Herbès, J. M. (1999). Niger tiger bush as a natural water harvesting system. *Catena*, *37*(1–2), 231–256. https://doi.org/10.1016/S0341-8162(98)00061-7

Verbesselt, J., Umlauf, N., Hirota, M., Holmgren, M., Van Nes, E. H., Herold, M., Zeileis, A., & Scheffer, M. (2016). Remotely sensed

resilience of tropical forests. *Nature Climate Change*, *6*(11), 1028–1031. https://doi.org/10.1038/nclimate3108

SUPPORTING INFORMATION

Additional supporting information may be found in the online version of the article at the publisher's website.

How to cite this article: Buxton, J. E., Abrams, J. F., Boulton, C. A., Barlow, N., Rangel Smith, C., Van Stroud, S., Lees, K. J., & Lenton, T. M. (2021). Quantitatively monitoring the resilience of patterned vegetation in the Sahel. *Global Change Biology*, 00, 1–17. https://doi.org/10.1111/gcb.15939